https://doi.org/10.5194/egusphere-2024-2956
Preprint. Discussion started: 8 October 2024

Investigation of the occurrence of significant deviations in the magnetopause location: Solar wind and foreshock effects

Niklas Grimmich[1], Adrian Pöppelwerth[1], Martin Owain Archer[2], David Gary Sibeck[3], Ferdinand Plaschke[1], Wenli Mo[4], Vicki Toy-Edens[4], Drew Lawson Turner[4], Hyangpyo Kim[5], and Rumi Nakamura[5]

[1]Institut für Geophysik und Extraterrestrische Physik, Technische Universität Braunschweig, Braunschweig, Germany
[2]Department of Physics, Imperial College London, London, UK
[3]NASA Goddard Space Flight Center, Greenbelt, Maryland, USA
[4]Johns Hopkins University Applied Physics Laboratory, Laurel, Maryland, USA
[5]Space Research Institute, Austrian Academy of Sciences, Graz, Austria

Correspondence: Niklas Grimmich (n.grimmich@tu-braunschweig.de)

Abstract. The dynamic motion of the magnetopause, the boundary between the Earth's magnetic field and the interplanetary magnetic field, is mainly driven by pressure variations and changes in the interplanetary magnetic field. Common magnetopause models can predict the location of the magnetopause in response to upstream conditions from different sets of input parameters, including pressure and the interplanetary magnetic field. However, recent studies have shown that some effects of upstream conditions may still be poorly understood, as deviations between model and in situ observations beyond the expected scatter due to constant magnetopause motion are quite common. Using data from the three most recent multi-spacecraft missions to near-Earth space (Cluster, THEMIS and MMS), we investigate the occurrence of these large deviations in observed magnetopause crossings from common empirical models. By comparing the results from different models, we find that the occurrence of these events appears to be model independent, suggesting that some physical processes may be missing from the models. To find these processes, we test whether the deviant magnetopause crossings are statistically associated with foreshocks and/or different solar wind types and show that in at least 50% of cases the foreshock can be responsible for the large deviations in the magnetopause's location. In the case where the foreshock is unlikely to be responsible, two distinct classes of solar wind are found to occur most frequently in association with the occurrence of magnetopause deviations: the "fast" solar wind and the solar wind plasma associated with transients such as interplanetary coronal mass ejections. Therefore, the plasma conditions associated with these solar wind classes could be responsible for the occurrence of deviant magnetopause observations. Our results may help to develop new and more accurate models of the magnetopause, which will be needed, for example, to accurately interpret the results of the upcoming SMILE mission.

1 Introduction

The motion of the magnetopause (MP), the boundary between the Earth's magnetic field and the interplanetary magnetic field (IMF), is driven by pressure variations in the upstream solar wind, changes in the IMF and flow shear between the magnetospheric and shocked solar wind plasma (e.g., Sibeck et al., 1991, 2000; Shue et al., 1997; Plaschke et al., 2009a, b;

https://doi.org/10.5194/egusphere-2024-2956
Preprint. Discussion started: 8 October 2024

Dušík et al., 2010; Archer et al., 2024a). On the dayside, the boundary attempts to balance the dynamic, plasma (thermal) and magnetic (from the draped field lines) pressures of the shocked solar wind on the magnetosheath side and the magnetic pressure on the magnetospheric side, resulting in the MP changing shape and location in response to upstream condition changes but also to some internal processes (e.g., Shue and Chao, 2013; Archer et al., 2024b). Typically, higher solar wind total pressures cause the MP to move closer to Earth than its average position, while lower total pressures allow the magnetosphere to expand.

Under strong southward IMF conditions, magnetic reconnection occurs, where planetary field lines and IMF lines are reconfigured, allowing magnetic flux and energy to be transported around the magnetosphere (Levy et al., 1964; Paschmann et al., 1979, 2013). Due to dayside flux erosion (Aubry et al., 1970; Sibeck et al., 1991; Shue et al., 1997, 1998; Kim et al., 2024) and the transient flux transfer event (Elphic, 1995; Dorelli and Bhattacharjee, 2009; Fear et al., 2017) that result from patchy magnetic reconnection, the MP surface can be undulated and generally moves earthwards from its nominal position. This is due to a decrease in the magnetic field strength in the dayside magnetosphere due to the transport of flux to the nightside and an increase in the field-aligned current strength (e.g., Maltsev and Liatskii, 1975; Wing et al., 2002; Samsonov et al., 2024). As a result, the magnetic pressure balancing the solar wind pressure is weakened and the MP is pushed inward.

When the IMF is in quasi-radial configuration, i.e. when the IMF cone angle $\vartheta_{\mathrm{cone}}$ between the Earth-Sun line and the IMF vector is less than 30° to 45°, the MP is often found sunward of its nominal position (Fairfield et al., 1990; Merka et al., 2003; Suvorova et al., 2010; Dušík et al., 2010; Samsonov et al., 2012; Park et al., 2016; Grygorov et al., 2017).

The so-called foreshock is formed in an extended region upstream of the bow shock due to a fraction of solar wind particles being reflected at the bow shock and backstreaming along the IMF. As a result, the interaction of solar wind particles with these backstreaming particles excites plasma waves due to instabilities (e.g., Eastwood et al., 2005; Wilson, 2016). A foreshock is present in most IMF configurations, but in the case of radial IMF, the region forms at and in front of the bow shock nose and becomes most important for MP dynamics by modulating the solar wind-magnetosphere interaction, e.g. through the occurrence of foreshock transients (e.g., Sibeck et al., 1999; Turner et al., 2011; Archer et al., 2015; Grimmich et al., 2024c).

Another explanation for the expansion under quasi-radial IMF conditions comes from MHD theory and is the reduction and subsequent redistribution of the total pressure of the solar wind by the bow shock and magnetosheath, resulting in a lower pressure on the magnetosphere, mainly due to the weaker effect of the field line drape, allowing the MP to move outwards to compensate for the pressure changes (see Suvorova et al., 2010; Samsonov et al., 2012).

Empirical models of the MP (e.g. Fairfield, 1971; Sibeck et al., 1991; Shue et al., 1997, 1998; Boardsen et al., 2000; Chao et al., 2002; Lin et al., 2010; Nguyen et al., 2022a, b) aim to predict the average location of the MP with a given shape under different solar wind conditions. Thus, in response to the upstream conditions described above, global and quasi-static changes in the boundary can be predicted. However, the models cannot capture the more realistic evolution of the boundary under changing conditions, which leads to a constant motion of the MP, resulting in a natural scatter of model predictions compared to spacecraft observations.

The simplest models, such as Shue et al. (1997, 1998), assume a rotational symmetry that is only influenced by the solar wind dynamic pressure p_{dyn} and the IMF component B_z. More complex models, such as the Lin et al. (2010) or Nguyen et al. (2022a, b) models, assume a more asymmetric shape as basis, include terms describing the indention of the surface at high

https://doi.org/10.5194/egusphere-2024-2956
Preprint. Discussion started: 8 October 2024

latitudes caused by the cusp and take into account more parameters affecting the shape and location of the MP (e.g., dipole tilt, magnetic pressure, and IMF magnitude).

Although the use of more complex models improves the prediction accuracy for the MP location, all models still have inherent biases and similar errors around 1 R_E (e.g. Šafránková et al., 2002; Case and Wild, 2013; Staples et al., 2020; Aghabozorgi Nafchi et al., 2024). Apart from the inability to capture the constant motion around the mean location of the MP, these errors could have several causes. On the one hand, due to the inherently variable nature and spatial structure of the solar wind, which sometimes shows widely different conditions between measurements a few hundred km apart, the conditions measured at L1 (which are often used for MP modelling) may not affect the Earth as expected (Borovsky, 2018a; Burkholder et al., 2020). Several studies like Walsh et al. (2019), O'Brien et al. (2023) or Aghabozorgi Nafchi et al. (2024) have shown the problems associated with the propagation of the solar wind to Earth. On the other hand, the studies of Grimmich et al. (2023a, 2024b) have identified specific parameters (such as solar wind speed, IMF cone angle, Alfvén Mach number and plasma β) that seem to be responsible for the deviation of observed MP crossings from the MP models. It is therefore possible that besides the propagation problem important mechanisms in the interaction are not yet captured by the models.

For example, high solar wind speeds appear to lead to an anti-Earthward expansion and outward displacement of the MP from the predicted model location, which is based on the assumption that the higher dynamic pressure in these cases compresses the MP (Grimmich et al., 2023a, 2024b). The foreshock, is reported to become stronger (more wave activity and frequent occurrence of transient events) under high solar wind speed conditions (Chu et al., 2017; Vu et al., 2022; Zhang et al., 2022; Xirogiannopoulou et al., 2024). Thus, one of these missing mechanisms could be that the parameters affecting the MP at the Earth's surface are modified by the formation of the foreshock region upstream of the Earth's bow shock (e.g., Walsh et al., 2019).

Another point which needs to be considered is the interconnected nature of the solar wind parameters (e.g., Xu and Borovsky, 2015; Borovsky, 2018b). In general, the solar wind plasma can be categorised into several types with systematic differences in solar wind parameters. Most common classification schemes divide the solar wind plasma into three to four main types: coronal hole plasma, ejecta and streamer belt plasma, from which a subset called sector reversal region plasma is sometimes separated (see Xu and Borovsky, 2015; Borovsky, 2020, and references therein). The change between the types of solar wind plasmas then causes synchronous changes in the solar wind parameters (Borovsky, 2018b).

Therefore, the approach of Grimmich et al. (2023a) in identifying the influence of individual parameters responsible for deviations from the MP models may be too simple when trying to identify the origins of the deviations. Since Koller et al. (2024) showed that taking different solar wind types into account improves the classification of magnetosheath ion distributions, it is possible that looking at the response of the MP to different solar wind types will reveal some missing aspects in current models.

Building on the results of previous studies by Grimmich et al. (2023a, 2024b), in this study we investigate the relationship between the observed and modelled MP deviations in relation to the different solar wind types and quantify the extent to which the foreshock is responsible for the deviations.

https://doi.org/10.5194/egusphere-2024-2956
Preprint. Discussion started: 8 October 2024

2 Datasets and Methods

For our investigation we use the Grimmich et al. (2023b, 2024a) and Toy-Edens et al. (2024a) datasets, which collect observation times and locations of magnetopause crossings (MPCs) from the Cluster (Escoubet et al., 2001, 2021), the Time History of Events and Macro-scale Interactions during Substorms (THEMIS, Angelopoulos, 2008) and the Magnetospheric Multiscale (MMS, Burch et al., 2016) missions in the years between 2001 and 2024. For a comprehensive overview of these datasets, we recommend consulting the relevant publications (Grimmich et al., 2023a, 2024b; Toy-Edens et al., 2024b).

As the datasets from Grimmich et al. (2023b) and Toy-Edens et al. (2024a) only collected dayside events, we have to limit our investigation here to the dayside magnetosphere. Thus, we only use events from the three datasets if they are associated with a positive x component at the observation location in the aberrated Geocentric Solar Ecliptic (aGSE) coordinate system (for details on the coordinate system see, e.g., Laundal and Richmond, 2016). Furthermore, in the Grimmich et al. (2023b, 2024a) datasets, the crossings are associated with a probability value indicating how certain the identification of the MP in the observation is. We follow the recommendation of the publications and use only the crossings with probabilities above 0.75, which are considered well identified crossings.

Following the previous studies of Grimmich et al. (2023a, 2024b), we also use the high-resolution OMNI data (King and Papitashvili, 2005) at a cadence of 1 min to associate all crossings in the datasets with upstream conditions. We take averages from an 8-minute OMNI interval preceding each crossing, if no more than 3 data points are missing in that interval for all solar wind parameters. Otherwise, the crossing is not associated with any upstream data. For reference, we also use the 1 min OMNI data from time intervals in the years between 2001 and 2024 where at least one of the three missions is located on the dayside and could potentially observe MPC events.

Using the associated OMNI data, we calculate the difference between the observed MP position $\boldsymbol{r}_{\mathrm{MP}}$ (i.e. the spacecraft position during a magnetopause crossing) and the position predicted by an MP model $\boldsymbol{r}_{\mathrm{mod}}$, which we can use to identify events where the model cannot explain the observation. Figure 1 shows a simplified case in the $(x,\, z)$-plane of the near-Earth space geometry. Here, the simplest approach to calculating the deviation would be to use the zenith angle θ between $\boldsymbol{r}_{\mathrm{MP}}$ and the x axis to determine the location of the MP model $\boldsymbol{r}_{\mathrm{mod}}$. However, we can see in the sketch that if we consider the zenith angle θ' for the calculation of $\boldsymbol{r}_{\mathrm{mod}}$, we can determine a perpendicular deviation from the modelled MP surface to the observation point, which is basically the normal displacement of the model MP to the observed crossing. This perpendicular/normal deviation, as seen in the sketch, is shorter than the simple approach calculations and therefore a more physically meaningful and unbiased difference between $\boldsymbol{r}_{\mathrm{MP}}$ and $\boldsymbol{r}_{\mathrm{mod}}$.

To describe this physically meaningful difference in a 3D space, we consider all possible θ and φ angles and take the angles θ' and φ' which yield the smallest deviation from the observed MP location, even though these may not be the angles that describe the observed location. We minimise the term

$$\Delta r = |\boldsymbol{r}_{\mathrm{MP}} - \boldsymbol{r}_{\mathrm{mod}}(\theta, \varphi)|, \tag{1}$$

where φ is the azimuth angle between the projection of $\boldsymbol{r}$ in the $(y,\, z)$ plane and the positive z axis.

https://doi.org/10.5194/egusphere-2024-2956
Preprint. Discussion started: 8 October 2024

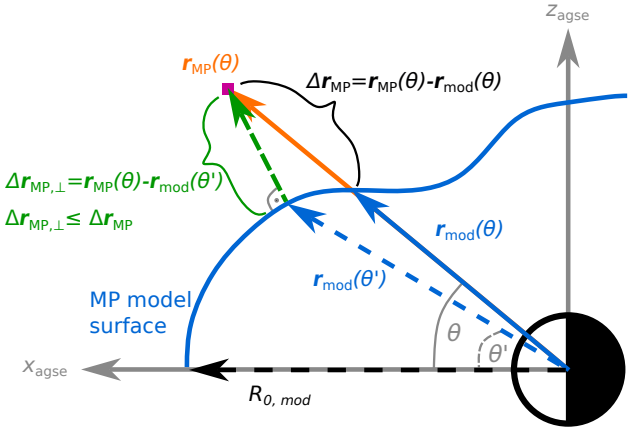

Figure 1. Visualisation of the deviation between r_{MP} and r_{mod}, an observed MP and the modelled MP location. The sketch is simplified and shows only the (x, z)-plane with an arbitrary (indented) MP model in blue. Including the azimuth angle φ next to the zenith angle θ would lead to the generalisation described in the text. It can be seen that the difference vector $\Delta \boldsymbol{r}_{\mathrm{MP}}$ between the spacecraft observation and the modelled surface of the MP would result in greater distances, when the using θ (the zenith angle of the spacecraft position) in model calculations. The shortest (minimum) distance along the normal to the surface can be found for the angle θ' (which can be different from θ) and gives a more physical meaningful representation of the deviation between model and observation (this would also be true for non-indented models).

By comparing the absolute values of $\boldsymbol{r}_{\mathrm{MP}}$ and $\boldsymbol{r}_{\mathrm{mod}}$, we can also see whether the observed location corresponds to a point further Earthward ($|\boldsymbol{r}_{\mathrm{MP}}| < |\boldsymbol{r}_{\mathrm{mod}}|$) or further anti-Earthward ($|\boldsymbol{r}_{\mathrm{MP}}| > |\boldsymbol{r}_{\mathrm{mod}}|$) than the model prediction. In the following, we refer to the events occurring further Earthward as compressed MPC and those occurring further anti-Earthward as expanded MPC. For example, the sketch in Figure 1 illustrates an expanded MPC.

In this study, we calculate the perpendicular deviation of the MP observation for two different MP models. We use the simple and widely used Shue et al. (1997, 1998) model, hereafter SH98, which describes the MP surface in a rotational symmetry with the function

$$r_{\mathrm{SH98}} = R_{0,\mathrm{SH98}} \left(\frac{2}{1+\cos\theta} \right)^{\alpha}, \tag{2}$$

where R_0 is the magnetopause stand-off distance and α the so-called flaring parameter. Since the SH98 model neglects asymmetries in the MP surface, the influence of the dipole tilt angle ψ on the MP shape, and also the prominent indentation feature associated with the cusp regions of the magnetosphere, we will also present results using the relatively new Nguyen et al. (2022b, a) model, hereafter N22b. This model incorporates the above features and is an extension of the SH98 model with its functional form described by

$$r_{\mathrm{N22b}} = R_{0,\mathrm{N22b}} \left(\frac{2}{1+\cos\theta} \right)^{\beta} (1 - q(\theta, \varphi, \psi)), \tag{3}$$

https://doi.org/10.5194/egusphere-2024-2956
Preprint. Discussion started: 8 October 2024

where $q(\theta, \varphi, \psi)$ is the term describing the indentation of the surface near the cusp influenced by the dipole tilt angle ψ. The flaring parameter of the N22b model β is also influenced by the dipole tilt.

We can use the minimisation of (1) with the vector $\boldsymbol{r}_{\mathrm{BS}}$ pointing to the surface of a bow shock model (instead of the vector pointing to an MP model surface) to obtain an estimate of the bow shock normal in the vicinity of the MPC observation. The vector $\Delta\boldsymbol{r}_{\perp} = \boldsymbol{r}_{\mathrm{MP}} - \boldsymbol{r}_{\mathrm{BS}}(\theta', \varphi')$ for the optimal combination of (θ', φ') from this new minimisation should then be roughly aligned with the normal of the model bow shock surface upstream of the MPC observation. Here we use the Chao et al. (2002) model (CH02) and therefore define the bow shock model normal associated with each MPC as

$$n_{\mathrm{BS}} = \frac{\boldsymbol{r}_{\mathrm{MP}} - \boldsymbol{r}_{\mathrm{CH02}}(\theta', \varphi')}{|\boldsymbol{r}_{\mathrm{MP}} - \boldsymbol{r}_{\mathrm{CH02}}(\theta', \varphi')|}. \tag{4}$$

We choose the sign of n_{BS} so that n_{BS} points to the sun (i.e. the x component is always positive).

The angle $\vartheta_{B,n}$ is defined as the angle between the computed normals n_{BS} and the IMF vector associated with the magnetopause observation. Typically, the region upstream of the quasi-parallel bow shock ($\vartheta_{B,n} < 45°$) is associated with the foreshock, while no foreshock activity is expected upstream of the quasi-perpendicular bow shock ($\vartheta_{B,n} > 45°$). However, the foreshock also extends into the quasi-perpendicular region, and in some cases $\vartheta_{B,n} < 60°$ is used to define the boundary of the active foreshock region (Wilson, 2016; Karlsson et al., 2021). The angle $\vartheta_{B,n}$ can therefore be used to estimate whether the crossing might be observed behind the quasi-parallel or quasi-perpendicular bow shock, and thus be associated with foreshock activity.

We are aware of the fact that this estimate of $\theta_{B,n}$ certainly does not give the angle at the bow shock from which the plasma came to influence the MP. Thus, our results in terms of foreshock activity could be improved with a more robust estimate of $\theta_{B,n}$. However, the overall errors in our estimates may not be significant, as the bow shock models are relatively blunt. Therefore, small deviations in the vector pointing to the optimal surface point responsible for the MP response would not result in vastly different angles.

In addition, we use the classification scheme introduced in Xu and Borovsky (2015) using the IMF magnitude $|\boldsymbol{B}_{\mathrm{IMF}}|$, the solar wind ion velocity $|\boldsymbol{u}_{\mathrm{sw}}|$, the solar wind ion density n_{ion} and the solar wind ion temperature T_{ion} to group the crossings according to the different solar wind types with empirically determined thresholds: ejecta (EJC), coronal hole origin (CHO), streamer belt origin (SBO), and sector reversal region (SRR) (see Xu and Borovsky, 2015). The threshold-based definition of the classes leads to problems near the class boundaries, which could lead to false classifications. However, we do not expect this to be a problem for the overall statistics we are interested in.

Transient phenomena such as interplanetary coronal mass ejections (ICMs) are associated with the EJC type, which is typically described by high IMF magnitudes, intermediate solar wind velocities, and low Alfvén Mach numbers and plasma βs. High solar wind speeds with intermediate IMF magnitudes, Alfvén Mach numbers and plasma β describe the CHO type solar wind (often referred to as the "fast" solar wind), which originates from open magnetic field lines in the solar corona (coronal holes). The SBO type (often referred to as the "slow" solar wind) originates from regions between the edge of coronal holes and streamer belts and can be described in terms of intermediate solar wind velocities, IMF magnitudes, Alfvén Mach numbers and plasma β. Finally, the SRR types (sometimes referred to as "very slow" solar wind) associated with the top of

https://doi.org/10.5194/egusphere-2024-2956
Preprint. Discussion started: 8 October 2024

Table 1. Median values with interquartile range of different solar wind plasma parameters in the four classes of solar wind plasma from Xu and Borovsky (2015). The parameter values are extracted from the OMNI dataset between the years 2001 and 2024.

	All sources	CHO plasma	SBO plasma	SRR plasma	EJC plasma
$\lvert\boldsymbol{B}_{\rm IMF}\rvert$ in nT	4.8 ± 2.9	5.2 ± 2.4	4.7 ± 2.5	3.8 ± 2.2	9.5 ± 4.9
$\lvert\boldsymbol{u}_{\rm sw}\rvert$ in kms^{-1}	408.2 ± 133.9	558.3 ± 106.1	408.9 ± 71.6	333.2 ± 46.4	403.5 ± 102.5
$\boldsymbol{n}_{\rm ion}$ in cm^{-3}	4.8 ± 4.5	2.8 ± 1.7	4.6 ± 3.0	8.4 ± 5.8	5.1 ± 5.7
$\boldsymbol{T}_{\rm ion}$ in 10^4K	6.5 ± 9.0	16.6 ± 10.4	7.1 ± 5.0	2.6 ± 1.7	3.9 ± 6.5
$\boldsymbol{p}_{\rm dyn}$ in nPa	1.7 ± 1.3	1.8 ± 1.3	1.6 ± 1.1	1.8 ± 1.4	1.7 ± 1.8
M_A	9.4 ± 4.8	9.0 ± 3.6	9.3 ± 3.9	12.4 ± 6.6	4.9 ± 1.7
β	1.7 ± 1.9	1.3 ± 0.91	1.8 ± 1.4	3.6 ± 4.1	0.4 ± 0.3

The parameters $\boldsymbol{p}_{\rm dyn}$, M_A and β are derived variables and therefore inherently connnected to the the four paramters $\lvert\boldsymbol{B}_{\rm IMF}\rvert$, $\lvert\boldsymbol{u}_{\rm sw}\rvert$, $\boldsymbol{n}_{\rm ion}$, $\boldsymbol{T}_{\rm ion}$.

helmet streamers, which are cusp-like magnetic loops in the solar corona, can best be described with low solar wind velocities and IMF magnitudes and high Alfvén Mach numbers and plasma β (see Xu and Borovsky, 2015; Borovsky, 2018b, 2020; Koller et al., 2024, and references therein). Table 1 shows the mean and median values for different solar wind parameters extracted from our OMNI data selection, falling into the four classes to further quantify the above descriptions.

Since the classification scheme of Xu and Borovsky (2015) did not include information about the orientation of the IMF, which is an important factor for the response of the MP, we extended the four categories to include information about non-radial northward ($\vartheta_{\rm cone} > 30°$ and $|\vartheta_{\rm clock}| < 90°$), non-radial southward ($\vartheta_{\rm cone} > 30°$ and $|\vartheta_{\rm clock}| > 90°$), and quasi-radial IMF ($\vartheta_{\rm cone} < 30°$). This gives a total of 12 different solar wind categories that can be associated with MPC observations.

3 Results

In the following, we only consider the crossing events from the three datasets in our analysis if all relevant parameters are determined, i.e. if we have values for $\Delta\boldsymbol{r}_{\perp,\rm SH98}$, $\Delta\boldsymbol{r}_{\perp,\rm N22b}$, $\vartheta_{B,n}$ and a classification results from the Xu and Borovsky (2015) scheme. This leaves us with 129,540 crossing events in a combined dataset to examine. The exact composition of this combined MPC dataset from the three missions can be found in the table 2.

Panel (a) and (b) of Fig. 2 show the distributions of $\Delta r_\perp$, the deviation between the observation and the models being considered. In order to eliminate any orbital bias in the histogram, we used the dwell time of the spacecraft in each bin for normalisation. Here the dwell time should be seen as the time during which the spacecraft are within the different bins (i.e. between certain ranges of model deviations) and can potentially observe an MPC with the associated model deviation. The normalisation therefore provides a more realistic distribution of the occurrence of MPC deviations, as MPCs found in regions frequently visited by the spacecraft are reduced in importance.

https://doi.org/10.5194/egusphere-2024-2956
Preprint. Discussion started: 8 October 2024

Table 2. Number of usable MPCs in the three datasets divided into separate subsets for different magnetospheric regions. The regions are divided according to the latitude and longitude angle (see text for details) in the equatorial subsolar region, the high latitude subsolar region, the equatorial flank regions and the high latitude flank regions. The table also gives a comparison between compressed and expanded MPCs in each dataset and subset. The expanded and compressed MPCs are identified for two different MP models (SH98 and N22b).

	THEMIS MPCs		Cluster MPCs		MMS MPCs		Total MPCs	
	comp.	exp.	comp.	exp.	comp.	exp.	comp.	exp.
Equat. subsol.	29,055		638		9,051		38,744	
deviant from SH98	143	1,893	7	59	119	920	269	2,872
deviant from N22b	78	3,442	—	84	100	1,174	178	4,700
High lat. subsol.	—		1,317		729		2,046	
deviant from SH98	—	—	544	7	68	19	612	26
deviant from N22b	—	—	46	134	28	43	74	177
Equat. flanks	62,588		3,117		18,082		83,787	
deviant from SH98	4,622	2,093	176	481	2,848	510	7,646	3,084
deviant from N22b	1,643	5,765	54	896	1,558	1,476	3,255	8,137
High lat. flanks	—		3,347		1,616		4,963	
deviant from SH98	—	—	1,206	110	542	—	1,748	110
deviant from N22b	—	—	121	561	214	46	335	607
Total	91,646		8,419		29,478		129,540	
deviant from SH98	4,765	3,986	1,933	657	3,577	1,449	10,275	6,092
deviant from N22b	1,721	9,207	222	1,675	1,900	2,739	3,843	13,621

Both distributions show a similar width according to a Gaussian fit we applied to the distributions, which gives a Full Width at Half Maximum (FWHM) value of 2.09 (2.07) R_E for the SH98 (N22b) model. Thus we can identify quite a few crossings with $|\Delta r_\perp| > 1.5\ R_E$ where the observed location differs from the predicted one in both distributions (cyan and red coloured events). For the SH98 model, 12.6% of the events are ever compressed or expanded MPCs, and for the N22b model, 13.5% are deviant MPCs. However, an important difference between the distributions is the mean: 0.05 R_E for the SH98 model and 0.5 R_E for the N22b model. This leads to the fact that the N22b model, when compared to the SH98 distribution, has significantly more expanded MPCs.

In a next step, we separate the distributions from Fig. 2a and b into four distinct regions of the magnetopause over the aGSE latitude ϕ and longitude λ: (1) subsolar crossings observed in the region where $|\lambda| < 30°$ and $|\phi| < 30°$; (2) high latitude subsolar crossings observed in the region where $|\lambda| < 30°$ and $|\phi| \geq 30°$; (3) near-equatorial flank crossings observed in the

https://doi.org/10.5194/egusphere-2024-2956
Preprint. Discussion started: 8 October 2024

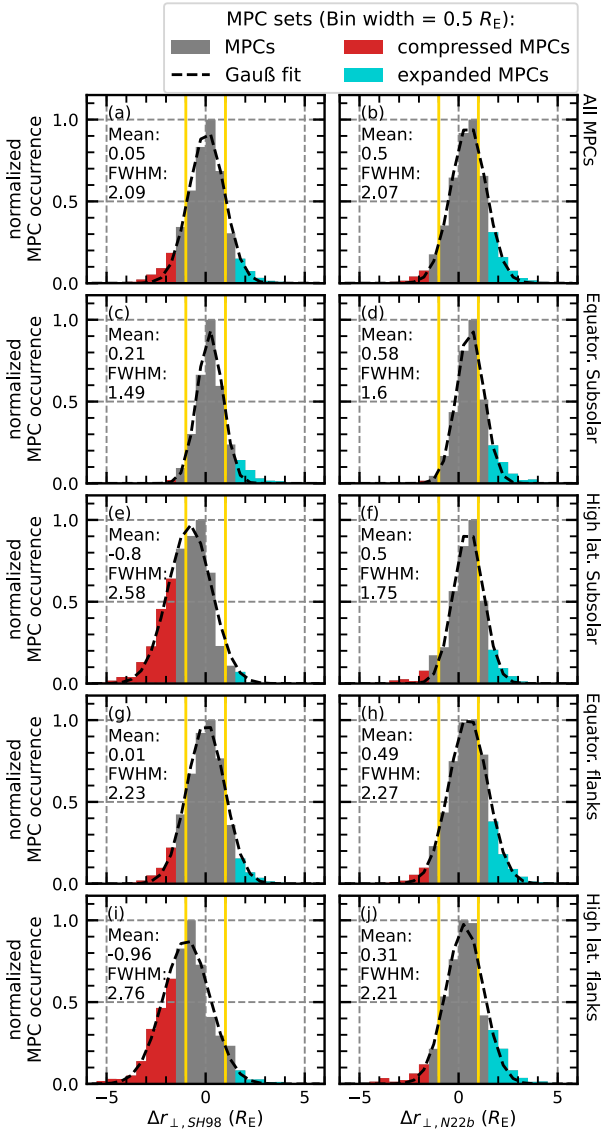

Figure 2. Distributions of $\Delta \boldsymbol{r}_{\perp}$ between the observations in the combined datasets and the prediction of the SH98 model in panel (a) and the prediction of the N22b model in panel (b). The distribution from (a) and (b) are split into subsets: (c) and (d) show the distributions for the subsolar magnetopause; (e) and (f) the high latitude MP in the noon sector; (g) and (h) the flank MP observations in the equatorial plane; (i) and (j) the flank MP observations in the high latitudes. The yellow lines represent the reported 1 R_E uncertainty of the MP models. The coloured regions of the histograms are the MPCs that clearly deviate from the selected model in the data set (see text for details). The dashed black lines represent a Gaussian fit to the histograms, with the mean and full width at half maximum (FWHM) of the fits also shown. The normalisation of the distribution is done first by dividing by the spacecraft dwell time in each bin and second by scaling the distribution to the maximum occurrence rate.

https://doi.org/10.5194/egusphere-2024-2956
Preprint. Discussion started: 8 October 2024

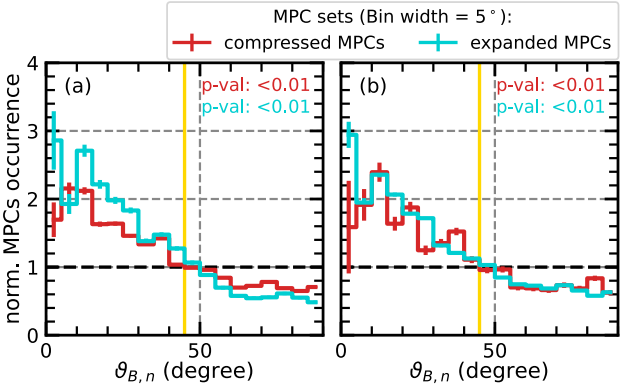

Figure 3. The $\vartheta_{B,n}$ distributions for the compressed and expanded MPCs deviant from the SH98 (a) and N22b (b) model are shown in red and cyan, respectively. The distributions are normalised by dividing by the total number of different $\vartheta_{B,n}$ values. A value of one in the plots (black dashed line) would therefore indicate that the occurrence of deviant MPCs is identical to the total occurrence, while values greater than one indicate that deviant MPCs occur more frequently under these conditions. The yellow lines mark the boundary between the quasi-parallel and the quasi-perpendicular foreshock condition associated with $\vartheta_{B,n}$. In addition, we show in each panel for the subsets the p-value that results from a Mann-Whitney U test: values less than 0.05, which is the case here, indicate statistically significant deviations from the reference distribution.

region where $|\lambda| \geq 30°$ and $|\phi| < 30°$ holds; (4) high-latitude flank crossings observed in the region where $|\lambda| \geq 30°$ and $|\phi| \geq 30°$ holds. The total number of MPCs observed in these regions can again be found in table 2.

Figure 2c-j show the regional separated distributions of $\Delta r_\perp$. There are a few things worth noting. In both figures it is clear that the distributions for the flank regions (panels (g)-(j)) are broader than the distributions for the two subsolar regions (panels (c)-(f)). In general, the distribution for the equatorial subsolar region with a FWHM value of 1.49 (1.6) R_E, considering the SH98 (N22b) model, shows the narrowest distribution with mostly expanded MPCs outside the error bounds of the model prediction. The distribution for the deviation from the SH98 model are shifted to negative deviations in the high latitude regions (cf. 2e and i), resulting in a lots of compressed MPCs in these subsets. Since the SH98 model does not include a cusp indentation, the encounter of the cusp in the high latitude regions causes a bias towards compressed MPCs in the $\Delta r_\perp$ distribution, which is clearly visible here and was reported by Grimmich et al. (2024b) for the Cluster dataset used here. The N22b model includes an indention term for the cusp, and we can see in Fig. 2f and j that this results in a narrower distribution with drastically fewer compressed MPCs. However, we can also see the shift towards positive deviations of $\Delta r_\perp$ in all regions for the N22b model, which of course also reduces the amount of observed compressed MPCs in the high latitudes.

Since we calculate an estimate for $\vartheta_{B,n}$ of the bow shock for each MPC, we can show here which bow shock configuration (quasi-parallel for $\vartheta_{B,n} < 45$, quasi-perpendicular for $\vartheta_{B,n} > 45$) is favourable for the occurrence of deviant MPCs.We identify favourable conditions, similar to the favourable solar wind conditions identified by Grimmich et al. (2023a, 2024b) for the THEMIS and Cluster data sets. We compare the occurrence of $\vartheta_{B,n}$ associated with compressed and expanded MPCs with the total occurrence of different bow shock configurations over the cause of the three missions.

https://doi.org/10.5194/egusphere-2024-2956
Preprint. Discussion started: 8 October 2024

Figure 3 again compares the result for the two different models. The distributions of $\vartheta_{B,n}$ associated with the outlying MPCs have been normalised by dividing these distributions by the reference distribution, which includes all times when a given $\vartheta_{B,n}$ value is observed and is not restricted to times when MPCs are observed. Thus, a value of one in the plots indicates that the overall distribution and that associated with the compressed/expanded MPCs are the same, and we can identify favourable conditions by looking for areas where we see values above one. In order to be sure that the observed deviations are statistically significant and not due to chance, we performed a Mann-Whitney U test, a generalisation of Student's t-test for non-normal distributions like ours (Mann and Whitney, 1947). If, for our null hypothesis that the underlying distribution of deviant events is the same as the underlying distribution of the reference, the probability of the test statistic being as deviant or more deviant by chance exceeds 5 %, we would discard our results as not significant. However, the test results in probability values well below 0.01, thus confirming the visible deviations from the reference as significant.

We can clearly see that for both models and for both the occurrence of compressed and expanded MPCs $\vartheta_{B,n} < 45°$ are favourable conditions. Thus, MPCs behind the quasi-parallel bow shock where a foreshock has developed tend to deviate more from the MP observation. In addition, we can extract from our data set that 51% (50%) of the MPCs deviating from the SH98 (N22b) model predictions are associated with the quasi-parallel bow shock conditions and likely foreshock activity, and 16% (17%) of the observed MPCs associated with $\vartheta_{B,n} < 45$ deviate from the SH98 (N22b) model prediction. Considering that $\vartheta_{B,n} < 60°$ is also sometimes used to define the boundary of the active foreshock region (Wilson, 2016; Karlsson et al., 2021), about 69% of the deviant MPCs might be associated with foreshock activity.

Since we know that under quasi-parallel conditions the MP can be highly disturbed and the occurrence of deviant MPCs in both directions (compressed and expanded MPCs) is likely, we look again at the $\Delta r_\perp$ distribution in different regions to see if the conditions in one region have a particular influence. Figure 4 shows, for the SH98 and N22b models respectively, the comparison of the distributions of $\Delta r_\perp$ associated with quasi-parallel and quasi-perpendicular conditions for all MPCs and in the four MP regions defined above.

Figure 4a and b show a visible effect of the presence of the foreshock region on the general $\Delta r_\perp$ distributions, with shifts in the mean and broadening of the distributions. Specifically, the bow shock condition seems to have the largest effect on the subsolar region. This is somewhat to be expected, as the MP in this case is immediately downstream of the foreshock, which is not the case at higher latitudes. Both in Fig. 4c and d we notice a shift towards larger positive deviation from the model predictions if the MPCs are associated with quasi-parallel conditions; the mean value of the Gaussian fit for the SH98 (N22b) model distribution shifts from 0.16 (0.52) R_E to 0.34 (0.72) R_E when the MPCs are associated with quasi-parallel conditions. We can also see that the quasi-parallel distribution is significantly wider compared to the quasi-perpendicular distribution in the sub-solar region (cf. FWHM values in panel (c)), indicating an increased variability of the MP location, e.g. due to more frequent motion.

Although we see a slight broadening of the $\Delta r_\perp$ distribution associated with low $\vartheta_{B,n}$ values for both models in the flank and high latitude regions (panels (e) to (j)), accompanied by a shift in the distribution, the influence is not as pronounced. At the flanks the quasi-parallel distributions shift by about 0.1 R_E towards negative deviations, while at the high latitude subsolar MP the shift is about 0.07 R_E towards positive deviations.

https://doi.org/10.5194/egusphere-2024-2956
Preprint. Discussion started: 8 October 2024

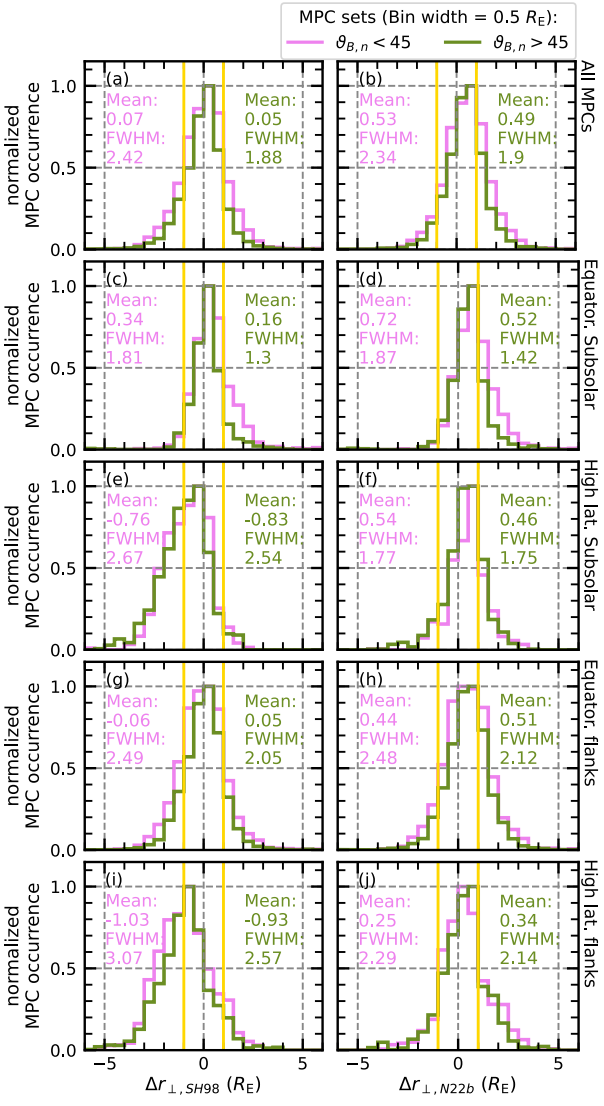

Figure 4. Comparison of $\Delta r_\perp$ distributions of MPCs associated with different $\vartheta_{B,n}$ in different magnetospheric regions. As before in Fig. 2, panels (a) and (b) show the distributions that include all of the MPC observations; (c) and (d) show the distributions for the subsolar magnetopause; panel (e) and(f) the high latitude MP in the noon sector; panel (g) and (h) the flank MP observation in the equatorial plane; panel (i) and(j) the flank MP observation in the high latitudes. The violet distributions belong to MPCs associated with $\vartheta_{B,n} < 45°$ and therefore observed behind a quasi-parallel foreshock region, while the green distributions belong to MPCs associated with $\vartheta_{B,n} > 45°$. For each distribution, the mean and full width at half maximum (FWHM) values of a associated Gaussian fit are also displayed and the yellow line mark the reported 1 R_E uncertainty of the MP model.

However, if we look at the dawn and dusk flanks separately, we find a general asymmetry in the $\Delta r_\perp$ distributions (see Fig. 5): In the equatorial plane (panels (a)-(d)), the distributions on the dusk flank are narrower with a mean at positive deviations,

https://doi.org/10.5194/egusphere-2024-2956
Preprint. Discussion started: 8 October 2024

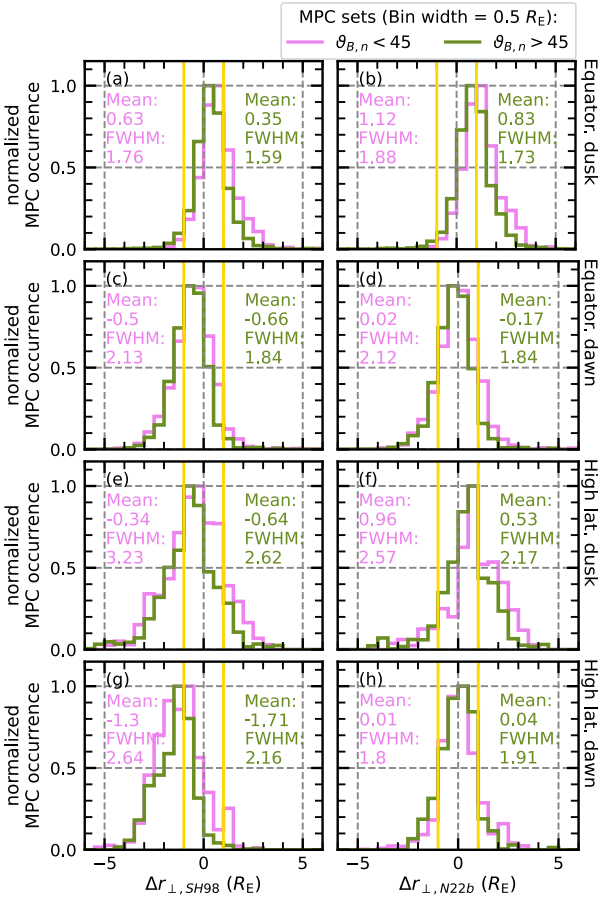

Figure 5. Comparison of $\Delta r_\perp$ distributions of MPCs associated with different $\vartheta_{B,n}$ on the dawn and dusk flanks. Panels (a) and (b) show the distributions for the equatorial dusk flank MPC observations; (c) and (d) show the distributions for the equatorial dawn flank; panels (e) and (f) the high latitude MP at the dusk flank; panels (g) and (h) the high latitude MP at the dawn flank. The violet distributions similar to Fig. 4 belong to MPCs associated with $\vartheta_{B,n} < 45°$, while the green distributions belong to MPCs associated with $\vartheta_{B,n} > 45°$. For each distribution, the mean and full width at half maximum (FWHM) values of an associated Gaussian fit are also shown, and the yellow lines mark the reported 1 R_E uncertainty of the MP model.

whereas the distributions on the dawn flank are wider with a mean shifted towards negative deviations. While at high latitudes (panels (e)-(h)) the shift of the means between dawn (more towards negative deviations) and dusk (more towards positive deviations) is the same as at the equatorial latitudes, the width of the distributions is different, with wider distributions at high latitude dusk flanks and narrower distributions at high latitude dawn flanks. The shifts in the means indicate that, on average, the models tend to under-predict the location of the MP at dusk and over-predict the location of the MP at dawn.

In addition to these general observations on the dawn and dusk flanks, we can also see a similar widening of the distribution associated with foreshock activity (i.e. for $\vartheta_{B,n} < 45$) as in the other regions shown in Fig. 4. In the equatorial plane, the

https://doi.org/10.5194/egusphere-2024-2956
Preprint. Discussion started: 8 October 2024

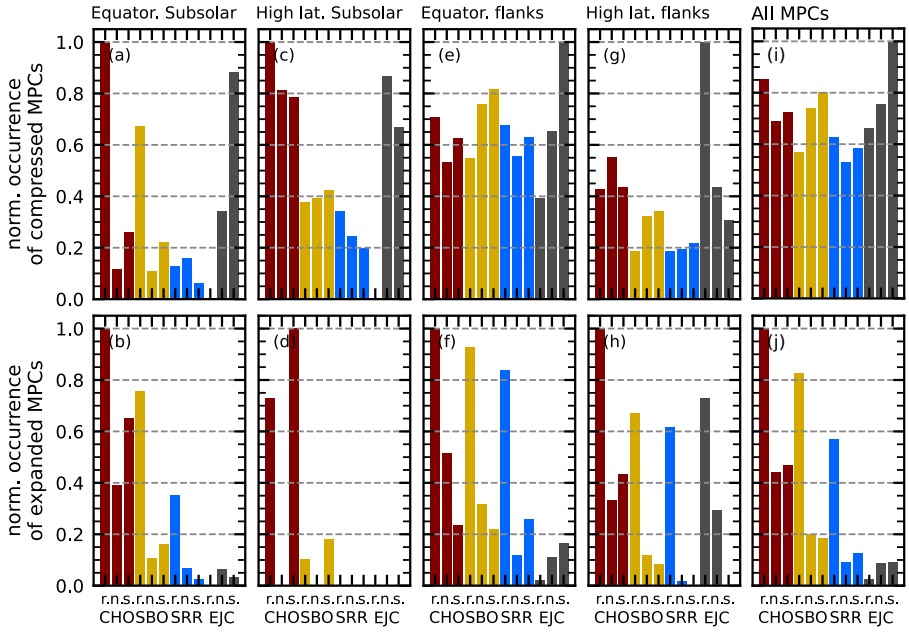

Figure 6. Comparison of the occurrence of compressed MPCs (top panels) and expanded MPCs (bottom panels) deviant from the SH98 model for different solar wind plasma conditions. The solar wind conditions are grouped according to the classification scheme of Xu and Borovsky (2015), with different colours corresponding to different solar wind types: red for coronal hole origin (CHO), yellow for streamer belt origin (SBO), blue for sector reversal region (SRR) and grey for ejecta (EJC). Each solar wind type is further divided into three subcategories corresponding to the IMF direction: quasi-radial IMF (r.), northward IMF (n.) and southward IMF (s.). Each bin is normalized by dividing the count rate of MPCs during a particular solar wind type by the count rate of that solar wind type in the OMNI data during the observation period, and then scaled to the maximum occurrence rate in each panel. Panels (a) and (b) show MPC events observed in subsolar region, panels (c) and (d) events observed in high latitude subsolar region, panels (e) and (f) show events observed in equatorial flank regions, panels (g) and (h) show events observed in high latitude flank regions and panels (i) and (h) show the combined MPC datasets events.

distributions on the dawn flanks widen almost twice as much as the distribution on the dusk flank when foreshock activity leads to more frequent deviations from model predictions due to the more turbulent motion of the MP surface behind a quasi-parallel bow shock. We can also see that although in Fig. 4(g) and (h) it looked as if the distributions were shifted towards negative deviations under quasi-parallel conditions, the separation in the dawn and dusk flank crossings revealed that at both flank crossings under the quasi-parallel conditions lead to a shift of the distributions towards positive deviations, similar to the effect seen in the subsolar region. The previously observed shift towards negative values is most likely a result of the asymmetry between the two flanks, as the dawn flank crossings are generally shifted towards these values and also have a stronger difference between quasi-parallel and quasi-perpendicular conditions.

Besides the influence of the bow shock configuration, which seems to correlate well with some of the observed deviations from model predictions, we also want to better determine the solar wind conditions responsible for the deviations. Since

https://doi.org/10.5194/egusphere-2024-2956
Preprint. Discussion started: 8 October 2024

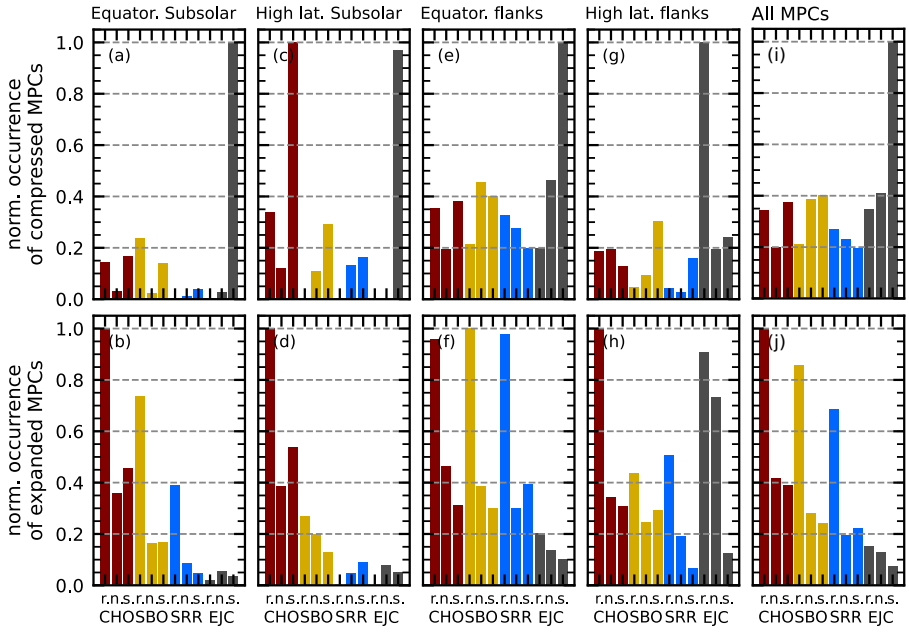

Figure 7. Comparison of the occurrence of compressed MPCs (top panels) and expanded MPCs (bottom panels) deviant from the N22b model for different solar wind plasma conditions, similar to Fig. 6.

we have associated each MPC with a corresponding solar wind plasma class, we can investigate the occurrence of deviant MPCs for a combination of solar wind parameters (instead of the single parameter influence investigated by Grimmich et al., 2023a, 2024b).

In Fig. 6 and 7 we show the normalized occurrence of compressed and expanded MPCs during the 12 different solar wind conditions we defined based on the Xu and Borovsky (2015) scheme in the different magnetospheric regions for both models. Normalization was performed by dividing each number of occurrences of a particular class associated with an MPC by the total number of occurrences of that class in the OMNI dataset between 2001 and 2024, before scaling the distribution in each panel to the maximum occurrence rate. While the relative abundance of classes for each panel is not affected by normalization, comparisons between panels must be made with caution, as the scaling for better visibility may distort the view on the importance of classes in different panels.

We see some clear dependencies for the occurrence of deviant MPCs (more or less independent of the model used to determine these MPCs): Compressed MPCs are clearly common for southward IMF orientations, with EJC plasma being quite prominent. However, we also see that SBO and CHO plasma are similarly abundant when compressed MPCs are observed (see Figs. 6i and 7i). Interestingly, the radial IMF seems to play a role especially in the high latitude flanks in the EJC plasma (panels (g)) and, according to the SH98 deviations, also in the subsolar region in the CHO plasma (Fig. 6a and c). Expanded MPCs occur most frequently under any radial IMF direction and most frequently during the CHO solar wind (see Fig. 6j and

https://doi.org/10.5194/egusphere-2024-2956
Preprint. Discussion started: 8 October 2024

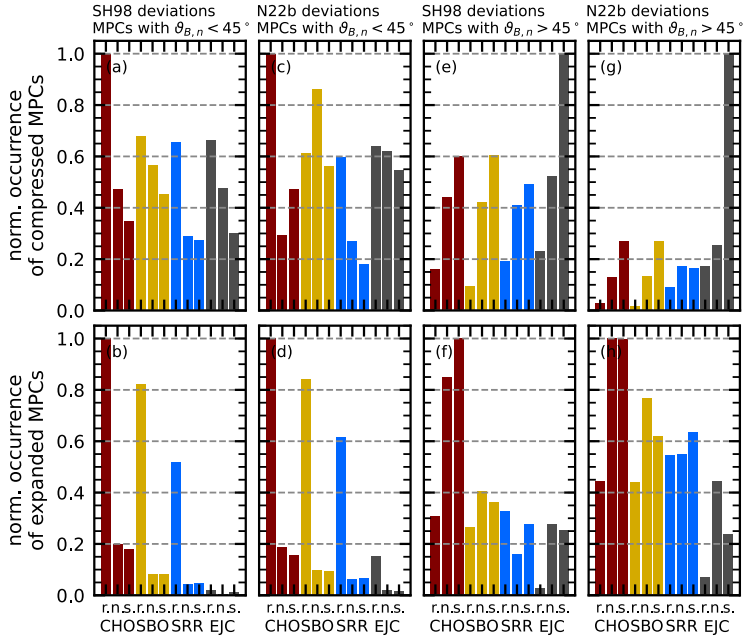

Figure 8. Comparison of the occurrence of compressed MPCs (top panels) and expanded MPCs (bottom panels) deviant from the SH98 and N22b MP models for different solar wind plasma conditions, similar to Fig. 6 and 7. Here, the occurrence of deviant MPCs associated with $\vartheta_{B,n} < 45^\circ$ (panels (a) and (b) for SH98 deviations and (e) and (f) for N22b deviations) is compared to the occurrence of deviant MPCs associated with $\vartheta_{B,n} > 45^\circ$ (panels (c) and (d) for SH98 deviations and (g) and (h) for N22b deviations).

7j). Although CHO dominates, SBO and SRR plasma become more important for expanded MPCs on the flank (panels (f) and (h)), while EJC solar wind plays almost seemingly only for high latitude flank crossings a role (panel (h)).

It should be noted that there are obvious differences between the results associated with the SH98 and N22b models (e.g. in panels (c) and (d)). However, these differences can easily be attributed to the lack of data for compressed and expanded MPCs associated with one or the other model in certain magnetospheric regions (see Table 2).

Similar to the $\Delta r_\perp$ distributions, we want to separate the distribution of the occurrence of deviant MPCs associated with different solar wind classes into MPCs behind a quasi-parallel and a quasi-perpendicular bow shock using $\vartheta_{B,n}$. Therefore, Fig. 8 shows the occurrence under the solar wind classes for MPCs with $\vartheta_{B,n} < 45^\circ$ and $\vartheta_{B,n} > 45^\circ$; the compressed and expanded MPCs are selected with the SH98 and N22b models, respectively. For both models we can again see similar characteristics for the occurrence of deviant MPCs.

We can see more clearly that for the compressed MPCs (top panels of Fig. 8) the southward IMF and EJC plasma is responsible for deviations behind quasi-perpendicular bow shock conditions, while radial IMF conditions within all plasma types occur often for the events behind the quasi-parallel bow shock. Furthermore, CHO plasma appears to be more important for the quasi-parallel conditions than for the quasi-perpendicular conditions. It also seems that SBO and CHO plasma types are similarly abundant only for compressed MPCs behind the quasi-perpendicular bow shock (see panels (e) and (g)).

https://doi.org/10.5194/egusphere-2024-2956
Preprint. Discussion started: 8 October 2024

For the expanded MPCs (bottom panels of Fig. 8) we see the importance of the CHO plasma for the occurrence independent of the bow shock conditions. We also see more clearly that radial IMF conditions could be mainly responsible for the expanded MPCs behind the quasi-parallel bow shock (see panels (b) and (d)). Overall, we can see that in 59% (57%) of the cases we encounter expanded MPCs that deviate from the SH98 (N22b) model behind a quasi-parallel bow shock, the IMF orientation is quasi-radial. Otherwise, it is interesting to note that southward IMF conditions (mostly in CHO plasma) seem to be quite common for expanded MPCS behind the quasi-perpendicular bow shock (see panels (f) and (h)).

4 Discussion

Our investigations aimed to better identify the reasons why the spacecraft-observed position of the MP surface can differ quite substantially from the empirical model predictions. We build on the results of Grimmich et al. (2023a, 2024b) and combine three large datasets of dayside MPCs, including data from the Cluster, THEMIS and MMS missions, to comprehensively examine the dayside MP over a wide range of longitudes and latitudes. However, the different sizes of the data sets and the orbital inclinations of the missions have the disadvantage that not all magnetospheric regions are covered equally, as can be seen in the table 2 which might affect occurrence rates. Nevertheless, the difference in orbits is also beneficial, as the bias of uneven coverage of annual solar wind conditions due to variations in spacecraft apogees causing misinterpretation of occurrence rates, as reported by Vuorinen et al. (2023), should be substantially reduced by combining the different data sets. Thus, our results from the combined dataset should overall be even better at revealing the influences of the solar wind on the position of the MP than previous studies using only a single mission dataset.

Another point that helps to generalise and understand the occurrence of deviant MPCs is that we have chosen to use two different empirical MP models to identify deviant boundary crossing events. The Shue et al. (1997, 1998) model is one of the simpler models and, despite its cavities, is widely used in the community (e.g., also in the previous studies of Grimmich et al., 2023a, 2024b) to represent the basic behaviour of the MP surface and therefore was include here. The Nguyen et al. (2022a, b) model claims to be one of the most accurate empirical models, including all kinds of observed asymmetries and also the important cusp indents in the high-latitude regions for MP surface modelling. As this model has not, to our knowledge, been validated on independent data, we have decided to include it here to see if it is indeed more accurate. Furthermore, the comparison of the two models has allowed us to see whether the occurrence of deviant MPCs is model dependent or whether there is a lack of fundamental physical understanding in the models.

Despite the fact that the two MP models used were developed on very different data sources and have different input parameters, the occurrence of model deviations and the associated conditions that may be responsible are very similar. Indeed, this seems to indicate systematic biases due to uncaptured physics in the models, although since the MP is almost always in motion, some scatter is to be expected and will remain even if the models can be improved by our results. Knowing this similarities, we will not separate the results from the models in the following discussion, but will try to combine the results into one general statement.

https://doi.org/10.5194/egusphere-2024-2956
Preprint. Discussion started: 8 October 2024

As shown in Fig. 2a and b, the distribution of the model deviation $\Delta r_\perp$ has an almost identical width of 2.09 R_E and 2.07 R_E, and for both models about 13% of the crossings are deviant MPCs, indicating that their general occurrence seems to be model independent. Since several studies (e.g., Šafránková et al., 2002; Case and Wild, 2013; Nguyen et al., 2022b; Aghabozorgi Nafchi et al., 2024) point out the similar errors of empirical modelling (in part due to the constant motion around an average location of the MP), this is not surprising. The obvious difference in the distribution of deviant MPCs between the two models (from the SH98 model we get more compressed MPCs, while the N22b model identifies more expanded MPCs; see table 2) stems probably from two sources: 1) The cusp encounters in the high latitude crossings observed by Cluster lead to a bias towards compressed MPCs for the non-indented SH98 model (see e.g., Boardsen et al., 2000; Šafránková et al., 2002, 2005; Grimmich et al., 2024b). 2) In general, the N22b model seems to under estimate the location of the MP surface for about 0.5 R_E and therefore has a clear bias towards extended MPCs. At the moment we are not sure where this is coming from.

Although, for example, Aghabozorgi Nafchi et al. (2024) suggests that the deviations between observations and models are primarily due to inaccurate propagation of solar wind parameters from the L1 point (measurement point of the OMNI dataset) to Earth, we may have found other but also adjacent possible explanations in this study. As Figs. 3, 4 and 5 show, MPCs associated with quasi-parallel bow shock conditions (i.e. $\vartheta_{B,n} < 45$) are quite often deviant crossing events. This suggests that the development of the foreshock region is an important factor in the occurrence of these events. The foreshock region strongly modifies the upstream solar wind conditions affecting the magnetosphere due to its turbulence, but also due to the occurrence of unpredictable transients (Walsh et al., 2019; Zhang et al., 2022). This nicely explains the discrepancies, as due to the foreshock modifications, the input to the models are not the conditions in the vicinity of the MP that determine the boundary position.

Here we propose that about 50-70% (depending on the limit of $\vartheta_{B,n}$ chosen for the foreshock activity) of the deviant cases in the combined dataset are associated with foreshock activity and therefore likely to be explained by the foreshock influence. This influence seems to be strongest for the subsolar MP, and we can estimate from comparing the means in Fig. 4c and d that the MP is on average 0.2 R_E more sunward for these MPCs associated with foreshock activity. In addition, for the equatorial flanks (Fig. 5(a)-(d)) we see an asymmetry between dawn and dusk: the MP under foreshock influences is on average about 0.28 R_E more anti-Earthward on the dusk flank and on average about 0.18 R_E more anti-Earthward on the dawn flank. Furthermore, the MP clearly shows more motion on the dawn flank under foreshock influence, as the distribution of model deviations is wider compared to the dusk flank.

However, not all MPCs associated with the quasi-parallel bow shock conditions are affected by the foreshock in an extreme way, only 16% of the crossings behind a foreshock can be identified as deviant MPCs, while in the other case the model predictions seem to agree with the observation and the foreshock might cause only a smaller amplitude motion around the mean location. Therefore, the presence of the foreshock does not guarantee the occurrence of deviant MPC.

By looking at the influences of the solar wind classes introduced by Xu and Borovsky (2015) on the occurrence of deviating MPCs, we can potentially identify and differentiate additional sources of deviations from the models. In the figures 6 to 8 we can see which solar wind parameter combinations are most likely to be present during the encounter with deviant MPCs.

A CHO plasma, described by high solar wind speeds and temperatures with low ion densities and intermediate IMF magnitudes (compared to the average parameter values from the OMNI data), is most often present when expanded MPCs occur.

https://doi.org/10.5194/egusphere-2024-2956
Preprint. Discussion started: 8 October 2024

Consistent with this finding, high solar wind speeds (independent from other parameters) have previously been reported to be favourable for the onset of (large) sunward MP deformation (Grimmich et al., 2023a, 2024b; Guo et al., 2024). However, our results allow us to be more precise in such a statement by including several parameters.

Another point often found in the literature is the expansion of the MP under quasi-radial IMF conditions (Merka et al., 2003; Suvorova et al., 2010; Samsonov et al., 2012; Park et al., 2016; Grygorov et al., 2017; Guo et al., 2024), and so this orientation is naturally often associated with expanded MPCs, which is also visible in our findings. In addition, our results show that the expanded MPCs that occur during quasi-radical IMF conditions are significantly more often associated with quasi-parallel bow shock conditions. Since, under radial IMF conditions, the foreshock develops directly in front of the bow shock nose, and thus most of the dayside magnetosphere would be behind a quasi-parallel bow shock, this observation is not surprising.

In combination with the likely presence of CHO plasma simultaneously with quasi-radial IMF our findings further emphasizes that, besides the "normal" turbulence influencing the MP, foreshock transients might often be responsible for the deviant MPCs. These transients occur more frequently in the foreshock under exactly these conditions (Chu et al., 2017; Vu et al., 2022; Zhang et al., 2022; Xirogiannopoulou et al., 2024) and several studies have already shown that the very different plasma parameters in the core of these transients can significantly deform the MP towards the Sun (e.g., Sibeck et al., 1999; Turner et al., 2011; Archer et al., 2015; Grimmich et al., 2024c). It is also worth noting that the foreshock developed in the CHO plasma should be further investigated. This could explain exactly why the MP appears to move globally outwards under radial IMF, which is most likely accompanied by CHO plasma. The composition of this plasma group could therefore be the dominant factor missing in the explanation.

Contrary to the finding of Grimmich et al. (2023a), which suggests that high Alfvén Mach numbers and solar wind plasma β are also important for the occurrence of extended MPCs, we find that the SRR plasma described by these conditions is less important and actually only relevant together with the radial IMF, which is likely to be the dominant effect for the occurrence of deviant MPCs. This shows that our classification of the solar wind and looking at the influences from a combined datasets helps to distinguish the more important mechanisms.

For the extended MPCs associated with quasi-perpendicular bow shock conditions, and therefore probably not caused by the foreshock modification, we see that besides northward CHO plasma, southward CHO plasma is mostly present during the observations. Since we see that this occurrence of southward CHO plasma is associated with the subsolar region at low and high latitudes (Figs. 6 and 7, panels (b) and (d)), one explanation for the expanded MPCs could be that large flux transfer events (Elphic, 1995; Dorelli and Bhattacharjee, 2009; Fear et al., 2017) resulting from ongoing reconnection at the MP nose under southward IMF lead to displacements of the MP surface. However, these results are largely due to the high latitude expanded MPCs, which are rather scarce in our dataset compared to the other regions. Therefore, there is no guarantee that our findings would hold up with more data points in these regions.

Another expected observation is the frequent presence of EJC plasma and southward IMF orientations during compressed MPCs, especially for events behind a quasi-perpendicular bow shock. EJC plasma described (compared to the average parameter values from the OMNI data) by high IMF magnitudes and intermediate solar wind velocities, densities and temperatures is associated with strong transient phenomena like ICMEs. Such ICMEs are known to cause geomagnetic storms (e.g., Denton

https://doi.org/10.5194/egusphere-2024-2956
Preprint. Discussion started: 8 October 2024

et al., 2006; Kilpua et al., 2017) in which the MP moves towards Earth. Similarly, it is well known that reconnection occurs during the southward IMF, leading to an MP found further Earthward (Levy et al., 1964; Paschmann et al., 1979; Sibeck et al., 1991; Shue et al., 1997, 1998; Paschmann et al., 2013). Therefore, compressed MPCs may be produced in both instances. Since we can infer that the occurrence of EJC plasma is slightly more likely than other types for southward IMF, the EJC plasma composition may be the dominant factor explaining the compressed MPCs.

EJC plasma is also associated with low Alfvén Mach numbers and plasma β caused by the high IMF magnitudes. Thus the results here showing that this type of plasma is favoured for the occurrence of compressed MPCs agree with the previous results from Grimmich et al. (2023a) claiming exactly this from the single parameter study. However, it is now clearer that the parameters are in fact related and in their combination responsible for the occurrence.

Looking at the compressed MPC associated with the foreshock activity, we see that in addition to the presence of the EJC plasma as the source, the radial IMF in the CHO plasma is important. This similar to the result for the expanded MPCs is most likely linked to the foreshock appearing in front of the MP nose and foreshock transient modulating the MP. In particular, the boundary compression regions of the transients (Schwartz, 1995; Turner et al., 2013; Liu et al., 2016) cause MP motion towards the Earth, which may result in compressed MPC observations.

In addition, the quasi-parallel domain of the bow shock is cited as the origin for the development of magnetosheath jets (Plaschke et al., 2018). Since they can lead to MP indention even under radial IMF conditions where the MP is expected to be more expanded (e.g. Shue et al., 2009; Wang et al., 2023; Yang et al., 2024; Němeček et al., 2023), they could be another explanation for the occurrence of compressed MPCs.

In general, we can also see that SBO plasma (the "normal"/"mean" solar wind) is often present during compressed MPC observations. Processes such as Kelvin-Helmholtz or surface waves, which occur independent from IMF orientations (Johnson et al., 2014; Kavosi and Raeder, 2015; Masson and Nykyri, 2018; Archer et al., 2019, 2024a), are possible explanations for these events, especially since most of the compressed MPCs more often associated with SBO plasma are observed on the flanks where Kelvin-Helmholtz instabilities are more likely.

Overall, the SW class analysis gives a very similar picture to the results of Grimmich et al. (2023a). However, it now seems clearer to what extent the foreshock, which is often overlooked when discussing errors in MP modelling, should be held responsible and in which region this phenomenon might be important for the occurrence of deviant MPCs.

Nevertheless, we would like to point out again that some regional results could be biased due to the few events observed, especially the high latitude regions would benefit from more events to further solidify the results obtained. The upcoming Solar Wind Magnetosphere Ionosphere Link Explorer (SMILE) mission (Branduardi-Raymont et al., 2018) will again be a near-Earth, polar-orbiting satellite, providing new in-situ observations of the high latitude MP in this region that could be used to reduce this potential bias.

Furthermore, the SMILE mission aims to observe and image the MP via X-ray observations and is in need of accurate MP models for its analysis techniques (see Kuntz, 2019; Wang and Sun, 2022). Our study can be seen as a first step towards developing a better empirical model that captures to some extent the effect presented here. An important point for such a future model could be a regional dependency, as we have seen that deviations are more common on the flanks, and the inclusion of

https://doi.org/10.5194/egusphere-2024-2956
Preprint. Discussion started: 8 October 2024

foreshock activity by including $\vartheta_{B,n}$. In addition, a more probabilistic approach to prediction of the MP surface under different input parameters may be beneficial.

5 Conclusions

In short, by combining data from different spacecraft missions that have collected MP observations over the last two decades, we have been able to identify model-independent conditions that occur during deviations between model predictions and spacecraft observations. The model deviations are present throughout the dayside magnetosphere, although regional dependencies are clearly visible. In the magnetospheric flanks the deviations are generally more frequent, especially the compressed MPCs, and the expanded MPCs seem to occur more frequently in the near equatorial plane.

We can clearly show that the foreshock is in many cases responsible for the occurrence of deviant MPCs, with the most pronounced effect in the subsolar region. The turbulent nature of the foreshock and the occurring transients lead to large displacements of the MP in earthward and anti-earthward directions, generally resulting in an average model deviation of 0.1 to 0.2 R_{E} anti-earthward. This also leads us to suspect that large amplitude surface and Kelvin-Helmholtz waves may be more common, and our results may often represent the resulting moving MP boundary. In future studies, we aim to investigate surface waves in relation the foreshock to see how the amplitude of the MP motion might change and whether this can explain some of the deviant MPCs.

Confirming and updating the results of Grimmich et al. (2023a), we further propose that compressed MPCs occur during southward IMFs embedded in a plasma of high IMF magnitudes caused by solar transients such as ICMEs, when foreshock activity is not a reasonable cause; compressed MPCs occur due to foreshock activity specifically for "fast" solar wind with radial IMF orientation; expanded MPCs generally occur most frequently for the "fast" solar wind, with foreshock activity responsible for deviations under radial IMF.

Overall, this study has identified processes that are still missing from commonly used MP models, and may help to improve these models in the future. However, as some of these identified processes may be associated with transient phenomena in the foreshock, which are inherently difficult to predict, this will be a challenging endeavour.

Data availability. The Open Science Framework (OSF) hosts the assembled MPC dataset by Grimmich et al. (2024a) for Cluster C1 and C3 at https://osf.io/pxctg/ and the dataset by Grimmich et al. (2023b) for THEMIS at https://osf.io/b6kux/. The dataset by Toy-Edens et al. (2024a) is available on Zenodo following https://zenodo.org/records/10491878. The OMNI data (King and Papitashvili, 2005) were obtained from the GSFC/SPDF OMNIWeb interface at https://spdf.gsfc.nasa.gov/pub/data/omni/omni_cdaweb/.

Author contributions. NG performed the analysis and wrote the original manuscript with additional input from AP and MOA. DGS together with FP was involved in developing the research idea for this study FP also provided the funding for this work. VTE, WM and DLT are part

https://doi.org/10.5194/egusphere-2024-2956
Preprint. Discussion started: 8 October 2024

of the development team of the MMS dataset and helped to integrate it into this work. AP, MOA, DGS, WM, FP, HK, RN, VTE and DLT all helped to discuss and finalise the manuscript.

Competing interests. The authors declare that the research was conducted in the absence of any commercial or financial relationships that could be construed as a potential conflict of interest.

Acknowledgements. The work of NG and FP on this study was supported by the German Center for Aviation and Space (DLR) under contract 50 OC 2401. AP was financially supported by the German Center for Aviation and Space (DLR) under contract 50 OC 2201. MOA was supported by UKRI (STFC/EPSRC) Future Leaders Fellowship MR/X034704/1. This research was supported by the International Space Science Institute (ISSI) in Bern, through ISSI International Team project #546 "Magnetohydrodynamic Surface Waves at Earth's Magnetosphere (and Beyond)". We thank Joe King and Natalia Papitashvili of the National Space Science Data Center (NSSDC) in the NASA/GSFC for the use of the OMNI 2 database. For the purpose of open access, the authors have applied a Creative Commons attribution (CC BY) licence to any Author Accepted Manuscript version arising.

https://doi.org/10.5194/egusphere-2024-2956
Preprint. Discussion started: 8 October 2024

References

Aghabozorgi Nafchi, M., Němec, F., Pi, G., Němeček, Z., Šafránková, J., Grygorov, K., Šimůnek, J., and Tsai, T. C.: Magnetopause location modeling using machine learning: inaccuracy due to solar wind parameter propagation, Frontiers in Astronomy and Space Sciences, 11, 1390427, https://doi.org/10.3389/fspas.2024.1390427, 2024.

Angelopoulos, V.: The THEMIS Mission, Space Sci. Rev., 141, 5–34, https://doi.org/10.1007/s11214-008-9336-1, 2008.

Archer, M. O., Turner, D. L., Eastwood, J. P., Schwartz, S. J., and Horbury, T. S.: Global impacts of a Foreshock Bubble: Magnetosheath, magnetopause and ground-based observations, Planetary and Space Science, 106, 56–66, https://doi.org/10.1016/j.pss.2014.11.026, 2015.

Archer, M. O., Hietala, H., Hartinger, M. D., Plaschke, F., and Angelopoulos, V.: Direct observations of a surface eigenmode of the dayside magnetopause, Nature Communications, 10, 615, https://doi.org/10.1038/s41467-018-08134-5, 2019.

Archer, M. O., Pilipenko, V. A., Li, B., Sorathia, K., Nakariakov, V. M., Elsden, T., and Nykyri, K.: Magnetopause MHD surface wave theory: progress & challenges, Frontiers in Astronomy and Space Sciences, 11, 1407172, https://doi.org/10.3389/fspas.2024.1407172, 2024a.

Archer, M. O., Shi, X., Walach, M.-T., Hartinger, M. D., Gillies, D. M., Di Matteo, S., Staples, F., and Nykyri, K.: Crucial future observations and directions for unveiling magnetopause dynamics and their geospace impacts, Frontiers in Astronomy and Space Sciences, 11, 1430099, https://doi.org/10.3389/fspas.2024.1430099, 2024b.

Aubry, M. P., Russell, C. T., and Kivelson, M. G.: Inward motion of the magnetopause before a substorm, Journal of Geophysical Research, 75, 7018, https://doi.org/10.1029/JA075i034p07018, 1970.

Boardsen, S. A., Eastman, T. E., Sotirelis, T., and Green, J. L.: An empirical model of the high-latitude magnetopause, Journal of Geophysical Research, 105, 23 193–23 220, https://doi.org/10.1029/1998JA000143, 2000.

Borovsky, J. E.: The spatial structure of the oncoming solar wind at Earth and the shortcomings of a solar-wind monitor at L1, Journal of Atmospheric and Solar-Terrestrial Physics, 177, 2–11, https://doi.org/10.1016/j.jastp.2017.03.014, 2018a.

Borovsky, J. E.: On the Origins of the Intercorrelations Between Solar Wind Variables, Journal of Geophysical Research (Space Physics), 123, 20–29, https://doi.org/10.1002/2017JA024650, 2018b.

Borovsky, J. E.: What magnetospheric and ionospheric researchers should know about the solar wind, Journal of Atmospheric and Solar-Terrestrial Physics, 204, 105271, https://doi.org/10.1016/j.jastp.2020.105271, 2020.

Branduardi-Raymont, G., Wang, C., C.P. Escoubet, C. P., Adamovic, M., Agnolon, D., Berthomier, M., Carter, J. A., Chen, W., Colangeli, L., Collier, M., Connor, H. K., Dai, L., Dimmock, A., Djazovski, O., Donovan, E., Eastwood, J. P., Enno, G., Giannini, F., Huang, L., Kataria, D., Kuntz, K., Laakso, H., Li, J., Li, L., Lui, T., Loicq, J., Masson, A., Manuel, J., Parmar, A., Piekutowski, T., Read, A. M., Samsonov, A., Sembay, S., Raab, W., Ruciman, C., Shi, J. K., Sibeck, D. G., Spanswick, E. L., Sun, T., Symonds, K., Tong, J., Walsh, B., Wei, F., Zhao, D., Zheng, J., Zhu, X., and Zhu, Z.: SMILE definition study report, European Space Agency, ESA/SCI, 1, 2018.

Burch, J. L., Moore, T. E., Torbert, R. B., and Giles, B. L.: Magnetospheric Multiscale Overview and Science Objectives, Space Sci. Rev., 199, 5–21, https://doi.org/10.1007/s11214-015-0164-9, 2016.

Burkholder, B. L., Nykyri, K., and Ma, X.: Use of the L1 Constellation as a Multispacecraft Solar Wind Monitor, Journal of Geophysical Research (Space Physics), 125, e27978, https://doi.org/10.1029/2020JA027978, 2020.

Case, N. A. and Wild, J. A.: The location of the Earth's magnetopause: A comparison of modeled position and in situ Cluster data, Journal of Geophysical Research (Space Physics), 118, 6127–6135, https://doi.org/10.1002/jgra.50572, 2013.

https://doi.org/10.5194/egusphere-2024-2956
Preprint. Discussion started: 8 October 2024

Chao, J. K., Wu, D. J., Lin, C. H., Yang, Y. H., Wang, X. Y., Kessel, M., Chen, S. H., and Lepping, R. P.: Models for the Size and Shape of the Earth's Magnetopause and Bow Shock, in: Space Weather Study Using Multipoint Techniques, edited by Lyu, L.-H., p. 127, Elsevier, https://doi.org/10.1016/S0964-2749(02)80212-8, 2002.

Chu, C., Zhang, H., Sibeck, D., Otto, A., Zong, Q., Omidi, N., McFadden, J. P., Fruehauff, D., and Angelopoulos, V.: THEMIS satellite observations of hot flow anomalies at Earth's bow shock, Annales Geophysicae, 35, 443–451, https://doi.org/10.5194/angeo-35-443-2017, 2017.

Denton, M. H., Borovsky, J. E., Skoug, R. M., Thomsen, M. F., Lavraud, B., Henderson, M. G., McPherron, R. L., Zhang, J. C., and Liemohn, M. W.: Geomagnetic storms driven by ICME- and CIR-dominated solar wind, Journal of Geophysical Research (Space Physics), 111, A07S07, https://doi.org/10.1029/2005JA011436, 2006.

Dorelli, J. C. and Bhattacharjee, A.: On the generation and topology of flux transfer events, Journal of Geophysical Research (Space Physics), 114, A06213, https://doi.org/10.1029/2008JA013410, 2009.

Dušík, Š., Granko, G., Šafránková, J., Němeček, Z., and Jelínek, K.: IMF cone angle control of the magnetopause location: Statistical study, Geophysical Research Letters, 37, L19103, https://doi.org/10.1029/2010GL044965, 2010.

Eastwood, J. P., Lucek, E. A., Mazelle, C., Meziane, K., Narita, Y., Pickett, J., and Treumann, R. A.: The Foreshock, Sapce Sci. Rev., 118, 41–94, https://doi.org/10.1007/s11214-005-3824-3, 2005.

Elphic, R. C.: Observations of Flux Transfer Events: A Review, Geophysical Monograph Series, 90, 225, https://doi.org/10.1029/GM090p0225, 1995.

Escoubet, C. P., Fehringer, M., and Goldstein, M.: Introduction The Cluster mission, Annales Geophysicae, 19, 1197–1200, https://doi.org/10.5194/angeo-19-1197-2001, 2001.

Escoubet, C. P., Masson, A., Laakso, H., Goldstein, M. L., Dimbylow, T., Bogdanova, Y. V., Hapgood, M., Sousa, B., Sieg, D., and Taylor, M. G. G. T.: Cluster After 20 Years of Operations: Science Highlights and Technical Challenges, Journal of Geophysical Research (Space Physics), 126, e29474, https://doi.org/10.1029/2021JA029474, 2021.

Fairfield, D. H.: Average and unusual locations of the Earth's magnetopause and bow shock, Journal of Geophysical Research, 76, 6700, https://doi.org/10.1029/JA076i028p06700, 1971.

Fairfield, D. H., Baumjohann, W., Paschmann, G., Luehr, H., and Sibeck, D. G.: Upstream pressure variations associated with the bow shock and their effects on the magnetosphere, Journal of Geophysical Research, 95, 3773–3786, https://doi.org/10.1029/JA095iA04p03773, 1990.

Fear, R. C., Trenchi, L., Coxon, J. C., and Milan, S. E.: How Much Flux Does a Flux Transfer Event Transfer?, Journal of Geophysical Research (Space Physics), 122, 12,310–12,327, https://doi.org/10.1002/2017JA024730, 2017.

Grimmich, N., Plaschke, F., Archer, M. O., Heyner, D., Mieth, J. Z. D., Nakamura, R., and Sibeck, D. G.: Study of Extreme Magnetopause Distortions Under Varying Solar Wind Conditions, Journal of Geophysical Research (Space Physics), 128, e2023JA031603, https://doi.org/10.1029/2023JA031603, 2023a.

Grimmich, N., Plaschke, F., Archer, M. O., Heyner, D., Mieth, J. Z. D., Nakamura, R., and Sibeck, D. G.: Database: THEMIS magnetopause crossings between 2007 and mid-2022, https://doi.org/10.17605/OSF.IO/B6KUX, 2023b.

Grimmich, N., Plaschke, F., Grison, B., Prencipe, F., Escoubet, C. P., Archer, M. O., Constantinescu, O. D., Haaland, S., Nakamura, R., Sibeck, D. G., Darrouzet, F., Hayosh, M., and Maggiolo, R.: Database: Cluster Magnetopause Crossings between 2001 and 2020, https://doi.org/10.17605/OSF.IO/PXCTG, 2024a.

https://doi.org/10.5194/egusphere-2024-2956
Preprint. Discussion started: 8 October 2024

Grimmich, N., Plaschke, F., Grison, B., Prencipe, F., Escoubet, C. P., Archer, M. O., Constantinescu, O. D., Haaland, S., Nakamura, R., Sibeck, D. G., Darrouzet, F., Hayosh, M., and Maggiolo, R.: The Cluster Spacecrafts' View Of The Motion Of The High-Latitude Magnetopause, Annales Geophysicae, 42, 371–394, https://doi.org/10.5194/angeo-42-371-2024, 2024b.

Grimmich, N., Prencipe, F., Turner, D. L., Liu, T. Z., Plaschke, F., Archer, M. O., Nakamura, R., Sibeck, D. G., Mieth, J. Z. D., Auster, H.-U., Constantinescu, O. D., Fischer, D., and Magnes, W.: Multi Satellite Observation of a Foreshock Bubble Causing an Extreme Magnetopause Expansion, Journal of Geophysical Research (Space Physics), 129, e2023JA032052, https://doi.org/10.1029/2023JA032052, 2024c.

Grygorov, K., Šafránková, J., Němeček, Z., Pi, G., Přech, L., and Urbář, J.: Shape of the equatorial magnetopause affected by the radial interplanetary magnetic field, Planetary and Space Science, 148, 28–34, https://doi.org/10.1016/j.pss.2017.09.011, 2017.

Guo, W., Tang, B., Zhang, Q., Li, W., Yang, Z., Sun, T., Ma, J., Zhang, X., Liu, Z., Guo, X., and Wang, C.: The Magnetopause Deformation Indicated by Fast Cold Ion Motion, Journal of Geophysical Research (Space Physics), 129, e2023JA032121, https://doi.org/10.1029/2023JA032121, 2024.

Johnson, J. R., Wing, S., and Delamere, P. A.: Kelvin Helmholtz Instability in Planetary Magnetospheres, Space Sci. Rev., 184, 1–31, https://doi.org/10.1007/s11214-014-0085-z, 2014.

Karlsson, T., Raptis, S., Trollvik, H., and Nilsson, H.: Classifying the Magnetosheath Behind the Quasi-Parallel and Quasi-Perpendicular Bow Shock by Local Measurements, Journal of Geophysical Research (Space Physics), 126, e29269, https://doi.org/10.1029/2021JA029269, 2021.

Kavosi, S. and Raeder, J.: Ubiquity of Kelvin-Helmholtz waves at Earth's magnetopause, Nature Communications, 6, 7019, https://doi.org/10.1038/ncomms8019, 2015.

Kilpua, E. K. J., Balogh, A., von Steiger, R., and Liu, Y. D.: Geoeffective Properties of Solar Transients and Stream Interaction Regions, Space SCi. Rev., 212, 1271–1314, https://doi.org/10.1007/s11214-017-0411-3, 2017.

Kim, H., Nakamura, R., Connor, H. K., Zou, Y., Plaschke, F., Grimmich, N., Walsh, B. M., McWilliams, K. A., and Ruohoniemi, J. M.: Localized Magnetopause Erosion at Geosynchronous Orbit by Reconnection, Geophysical Research Letters, 51, e2023GL107085, https://doi.org/10.1029/2023GL107085, 2024.

King, J. H. and Papitashvili, N. E.: Solar wind spatial scales in and comparisons of hourly Wind and ACE plasma and magnetic field data, Journal of Geophysical Research (Space Physics), 110, A02104, https://doi.org/10.1029/2004JA010649, 2005.

Koller, F., Raptis, S., Temmer, M., and Karlsson, T.: The Effect of Fast Solar Wind on Ion Distribution Downstream of Earth's Bow Shock, The Astrophysical Journal Letters, 964, L5, https://doi.org/10.3847/2041-8213/ad2ddf, 2024.

Kuntz, K. D.: Solar wind charge exchange: an astrophysical nuisance, The Astronomy and Astrophysics Review, 27, 1, https://doi.org/10.1007/s00159-018-0114-0, 2019.

Laundal, K. M. and Richmond, A. D.: Magnetic Coordinate Systems, Space Sci. Rev., 206, 27–59, https://doi.org/10.1007/s11214-016-0275-y, 2016.

Levy, R. H., Petschek, H. E., and Siscoe, G. L.: Aerodynamic aspects of the magnetospheric flow, AIAA Journal, 2, 2065–2076, https://doi.org/10.2514/3.2745, 1964.

Lin, R. L., Zhang, X. X., Liu, S. Q., Wang, Y. L., and Gong, J. C.: A three-dimensional asymmetric magnetopause model, Journal of Geophysical Research (Space Physics), 115, A04207, https://doi.org/10.1029/2009JA014235, 2010.

Liu, T. Z., Turner, D. L., Angelopoulos, V., and Omidi, N.: Multipoint observations of the structure and evolution of foreshock bubbles and their relation to hot flow anomalies, Journal of Geophysical Research (Space Physics), 121, 5489–5509, https://doi.org/10.1002/2016JA022461, 2016.

https://doi.org/10.5194/egusphere-2024-2956
Preprint. Discussion started: 8 October 2024

Maltsev, I. P. and Liatskii, V. B.: Field-aligned currents and erosion of the dayside magnetosphere, Planetary and Space Science, 23, 1257–1260, https://doi.org/10.1016/0032-0633(75)90149-X, 1975.

Mann, H. B. and Whitney, D. R.: On a test of whether one of two random variables is stochastically larger than the other, The annals of mathematical statistics, 18, 50–60, https://doi.org/10.1214/aoms/1177730491, 1947.

Masson, A. and Nykyri, K.: Kelvin-Helmholtz Instability: Lessons Learned and Ways Forward, Space Sci. Rev., 214, 71, https://doi.org/10.1007/s11214-018-0505-6, 2018.

Merka, J., Szabo, A., Šafránková, J., and Němeček, Z.: Earth's bow shock and magnetopause in the case of a field-aligned upstream flow: Observation and model comparison, Journal of Geophysical Research (Space Physics), 108, 1269, https://doi.org/10.1029/2002JA009697, 2003.

Nguyen, G., Aunai, N., Michotte de Welle, B., Jeandet, A., Lavraud, B., and Fontaine, D.: Massive Multi-Mission Statistical Study and Analytical Modeling of the Earth's Magnetopause: 4. On the Near-Cusp Magnetopause Indentation, Journal of Geophysical Research (Space Physics), 127, e29776, https://doi.org/10.1029/2021JA029776, 2022a.

Nguyen, G., Aunai, N., Michotte de Welle, B., Jeandet, A., Lavraud, B., and Fontaine, D.: Massive Multi-Mission Statistical Study and Analytical Modeling of the Earth's Magnetopause: 3. An Asymmetric Non Indented Magnetopause Analytical Model, Journal of Geophysical Research (Space Physics), 127, e30112, https://doi.org/10.1029/2021JA030112, 2022b.

Němeček, Z., Šafránková, J., Grygorov, K., Mokrý, A., Pi, G., Aghabozorgi Nafchi, M., Němec, F., Xirogiannopoulou, N., and Šimůnek, J.: Extremely Distant Magnetopause Locations Caused by Magnetosheath Jets, Geophysical Research Letters, 50, e2023GL106131, https://doi.org/10.1029/2023GL106131, 2023.

O'Brien, C., Walsh, B. M., Zou, Y., Tasnim, S., Zhang, H., and Sibeck, D. G.: PRIME: a probabilistic neural network approach to solar wind propagation from L1, Frontiers in Astronomy and Space Sciences, 10, 1250779, https://doi.org/10.3389/fspas.2023.1250779, 2023.

Park, J.-S., Shue, J.-H., Kim, K.-H., Pi, G., Němeček, Z., and Šafránková, J.: Global expansion of the dayside magnetopause for long-duration radial IMF events: Statistical study on GOES observations, Journal of Geophysical Research (Space Physics), 121, 6480–6492, https://doi.org/10.1002/2016JA022772, 2016.

Paschmann, G., Papamastorakis, I., Sckopke, N., Haerendel, G., Sonnerup, B. U. O., Bame, S. J., Asbridge, J. R., Gosling, J. T., Russel, C. T., and Elphic, R. C.: Plasma acceleration at the earth's magnetopause - Evidence for reconnection, Nature, 282, 243–246, https://doi.org/10.1038/282243a0, 1979.

Paschmann, G., Øieroset, M., and Phan, T.: In-Situ Observations of Reconnection in Space, Space Sci. Rev., 178, 385–417, https://doi.org/10.1007/s11214-012-9957-2, 2013.

Plaschke, F., Glassmeier, K. H., Auster, H. U., Angelopoulos, V., Constantinescu, O. D., Fornaçon, K. H., Georgescu, E., Magnes, W., McFadden, J. P., and Nakamura, R.: Statistical study of the magnetopause motion: First results from THEMIS, Journal of Geophysical Research (Space Physics), 114, A00C10, https://doi.org/10.1029/2008JA013423, 2009a.

Plaschke, F., Glassmeier, K. H., Sibeck, D. G., Auster, H. U., Constantinescu, O. D., Angelopoulos, V., and Magnes, W.: Magnetopause surface oscillation frequencies at different solar wind conditions, Annales Geophysicae, 27, 4521–4532, https://doi.org/10.5194/angeo-27-4521-2009, 2009b.

Plaschke, F., Hietala, H., Archer, M., Blanco-Cano, X., Kajdič, P., Karlsson, T., Lee, S. H., Omidi, N., Palmroth, M., Roytershteyn, V., Schmid, D., Sergeev, V., and Sibeck, D.: Jets Downstream of Collisionless Shocks, Space Sci. Rev., 214, 81, https://doi.org/10.1007/s11214-018-0516-3, 2018.

https://doi.org/10.5194/egusphere-2024-2956
Preprint. Discussion started: 8 October 2024

Samsonov, A., Milan, S., Buzulukova, N., Sibeck, D., Forsyth, C., Branduardi-Raymont, G., and Dai, L.: Time Sequence of Magnetospheric Responses to a Southward IMF Turning, Journal of Geophysical Research (Space Physics), 129, e2023JA032378, https://doi.org/10.1029/2023JA032378, 2024.

Samsonov, A. A., Němeček, Z., Šafránková, J., and Jelínek, K.: Why does the subsolar magnetopause move sunward for radial interplanetary magnetic field?, Journal of Geophysical Research (Space Physics), 117, A05221, https://doi.org/10.1029/2011JA017429, 2012.

Schwartz, S. J.: Hot flow anomalies near the Earth's bow shock, Advances in Space Research, 15, 107–116, https://doi.org/10.1016/0273-1177(95)00025-A, 1995.

Shue, J. H. and Chao, J. K.: The role of enhanced thermal pressure in the earthward motion of the Earth's magnetopause, Journal of Geophysical Research (Space Physics), 118, 3017–3026, https://doi.org/10.1002/jgra.50290, 2013.

Shue, J. H., Chao, J. K., Fu, H. C., Russell, C. T., Song, P., Khurana, K. K., and Singer, H. J.: A new functional form to study the solar wind control of the magnetopause size and shape, Journal of Geophysical Research, 102, 9497–9512, https://doi.org/10.1029/97JA00196, 1997.

Shue, J. H., Song, P., Russell, C. T., Steinberg, J. T., Chao, J. K., Zastenker, G., Vaisberg, O. L., Kokubun, S., Singer, H. J., Detman, T. R., and Kawano, H.: Magnetopause location under extreme solar wind conditions, Journal of Geophysical Research, 103, 17 691–17 700, https://doi.org/10.1029/98JA01103, 1998.

Shue, J. H., Chao, J. K., Song, P., McFadden, J. P., Suvorova, A., Angelopoulos, V., Glassmeier, K. H., and Plaschke, F.: Anomalous magnetosheath flows and distorted subsolar magnetopause for radial interplanetary magnetic fields, Geophysical Research Letters, 36, L18112, https://doi.org/10.1029/2009GL039842, 2009.

Sibeck, D. G., Lopez, R. E., and Roelof, E. C.: Solar wind control of the magnetopause shape, location, and motion, Journal of Geophysical Research, 96, 5489–5495, https://doi.org/10.1029/90JA02464, 1991.

Sibeck, D. G., Borodkova, N. L., Schwartz, S. J., Owen, C. J., Kessel, R., Kokubun, S., Lepping, R. P., Lin, R., Liou, K., Lühr, H., McEntire, R. W., Meng, C. I., Mukai, T., Němeček, Z., Parks, G., Phan, T. D., Romanov, S. A., Šafránková, J., Sauvaud, J. A., Singer, H. J., Solovyev, S. I., Szabo, A., Takahashi, K., Williams, D. J., Yumoto, K., and Zastenker, G. N.: Comprehensive study of the magnetospheric response to a hot flow anomaly, Journal of Geophysical Research, 104, 4577–4594, https://doi.org/10.1029/1998JA900021, 1999.

Sibeck, D. G., Kudela, K., Lepping, R. P., Lin, R., Němeček, Z., Nozdrachev, M. N., Phan, T. D., Prech, L., Šafránková, J., Singer, H., and Yermolaev, Y.: Magnetopause motion driven by interplanetary magnetic field variations, Journal of Geophysical Research, 105, 25 155–25 170, https://doi.org/10.1029/2000JA900109, 2000.

Staples, F. A., Rae, I. J., Forsyth, C., Smith, A. R. A., Murphy, K. R., Raymer, K. M., Plaschke, F., Case, N. A., Rodger, C. J., Wild, J. A., Milan, S. E., and Imber, S. M.: Do Statistical Models Capture the Dynamics of the Magnetopause During Sudden Magnetospheric Compressions?, Journal of Geophysical Research (Space Physics), 125, e27289, https://doi.org/10.1029/2019JA027289, 2020.

Suvorova, A. V., Shue, J. H., Dmitriev, A. V., Sibeck, D. G., McFadden, J. P., Hasegawa, H., Ackerson, K., Jelínek, K., Šafránková, J., and Němeček, Z.: Magnetopause expansions for quasi-radial interplanetary magnetic field: THEMIS and Geotail observations, Journal of Geophysical Research (Space Physics), 115, A10216, https://doi.org/10.1029/2010JA015404, 2010.

Toy-Edens, V., Mo, W., Raptis, S., and Turner, D. L.: 8 years of dayside magnetospheric multiscale (MMS) unsupervised clustering plasma regions classifications, https://doi.org/10.5281/zenodo.10491877, 2024a.

Toy-Edens, V., Mo, W., Raptis, S., and Turner, D. L.: Classifying 8 Years of MMS Dayside Plasma Regions via Unsupervised Machine Learning, Journal of Geophysical Research (Space Physics), 129, e2024JA032431, https://doi.org/10.1029/2024JA032431, 2024b.

https://doi.org/10.5194/egusphere-2024-2956
Preprint. Discussion started: 8 October 2024

Turner, D. L., Eriksson, S., Phan, T. D., Angelopoulos, V., Tu, W., Liu, W., Li, X., Teh, W. L., McFadden, J. P., and Glassmeier, K. H.: Multispacecraft observations of a foreshock-induced magnetopause disturbance exhibiting distinct plasma flows and an intense density compression, Journal of Geophysical Research (Space Physics), 116, A04230, https://doi.org/10.1029/2010JA015668, 2011.

Turner, D. L., Omidi, N., Sibeck, D. G., and Angelopoulos, V.: First observations of foreshock bubbles upstream of Earth's bow shock: Characteristics and comparisons to HFAs, Journal of Geophysical Research (Space Physics), 118, 1552–1570, https://doi.org/10.1002/jgra.50198, 2013.

Šafránková, J., Němeček, Z., Dusík, S., Prech, L., Sibeck, D. G., and Borodkova, N. N.: The magnetopause shape and location: a comparison of the Interball and Geotail observations with models, Annales Geophysicae, 20, 301–309, https://doi.org/10.5194/angeo-20-301-2002, 2002.

Šafránková, J., Dušík, Š., and Němeček, Z.: The shape and location of the high-latitude magnetopause, Advances in Space Research, 36, 1934–1939, https://doi.org/10.1016/j.asr.2004.05.009, 2005.

Vu, A., Liu, T. Z., Zhang, H., and Pollock, C.: Statistical Study of Foreshock Bubbles, Hot Flow Anomalies, and Spontaneous Hot Flow Anomalies and Their Substructures Observed by MMS, Journal of Geophysical Research (Space Physics), 127, e2021JA030029, https://doi.org/10.1029/2021JA030029, 2022.

Vuorinen, L., LaMoury, A. T., Hietala, H., and Koller, F.: Magnetosheath Jets Over Solar Cycle 24: An Empirical Model, Journal of Geophysical Research (Space Physics), 128, e2023JA031493, https://doi.org/10.1029/2023JA031493, 2023.

Walsh, B. M., Bhakyapaibul, T., and Zou, Y.: Quantifying the Uncertainty of Using Solar Wind Measurements for Geospace Inputs, Journal of Geophysical Research (Space Physics), 124, 3291–3302, https://doi.org/10.1029/2019JA026507, 2019.

Wang, C. and Sun, T.: Methods to derive the magnetopause from soft X-ray images by the SMILE mission, Geoscience Letters, 9, 30, https://doi.org/10.1186/s40562-022-00240-z, 2022.

Wang, X., Lu, J., Wang, M., Zhou, Y., and Hao, Y.: Simultaneous Observation of Magnetopause Expansion Under Radial IMF and Indention by HSJ, Geophysical Research Letters, 50, e2023GL105270, https://doi.org/10.1029/2023GL105270, 2023.

Wilson, L. B.: Low Frequency Waves at and Upstream of Collisionless Shocks, Washington DC American Geophysical Union Geophysical Monograph Series, 216, 269–291, https://doi.org/10.1002/9781119055006.ch16, 2016.

Wing, S., Sibeck, D. G., Wiltberger, M., and Singer, H.: Geosynchronous magnetic field temporal response to solar wind and IMF variations, Journal of Geophysical Research (Space Physics), 107, 1222, https://doi.org/10.1029/2001JA009156, 2002.

Xirogiannopoulou, N., Goncharov, O., Å afránková, J., and Němeček, Z.: Characteristics of Foreshock Subsolar Compressive Structures, Journal of Geophysical Research (Space Physics), 129, e2023JA032033, https://doi.org/10.1029/2023JA032033, 2024.

Xu, F. and Borovsky, J. E.: A new four-plasma categorization scheme for the solar wind, Journal of Geophysical Research (Space Physics), 120, 70–100, https://doi.org/10.1002/2014JA020412, 2015.

Yang, Z., Jarvinen, R., Guo, X., Sun, T., Koutroumpa, D., Parks, G. K., Huang, C., Tang, B., Lu, Q., and Wang, C.: Deformations at Earth's dayside magnetopause during quasi-radial IMF conditions: Global kinetic simulations and Soft X-ray Imaging, Earth and Planetary Physics, 8, 59–69, https://doi.org/10.26464/epp2023059, 2024.

Zhang, H., Zong, Q., Connor, H., Delamere, P., Facskó, G., Han, D., Hasegawa, H., Kallio, E., Kis, Á., Le, G., Lembège, B., Lin, Y., Liu, T., Oksavik, K., Omidi, N., Otto, A., Ren, J., Shi, Q., Sibeck, D., and Yao, S.: Dayside Transient Phenomena and Their Impact on the Magnetosphere and Ionosphere, Space Sci. Rev., 218, 40, https://doi.org/10.1007/s11214-021-00865-0, 2022.